A Three-Dimensional Model of Transport and Diffusion of Seeding Agents within Stratus

Yu Xing (余 兴), Dai Jin (戴 进)
Center of Weather Modification of Shaanxi Province, Xi'an 710015
Jiang Weimei (蒋维楣)
Department of Atmospheric Sciences, Nanjing University, Nanjing 210093
Fan Peng (樊 鹏)
Center of Weather Modification of Shaanxi Province, Xi'an 710015

(Received January 17, 2000; revised April 10, 2000)

ABSTRACT

It is essential to learn the temporal and spatial concentration distributions and variations of seeding agents in cloud seeding of precipitation enhancement. A three-dimensional puff trajectory model incorporating a mesoscale nonhydrostatic model has been formulated, and is applied to simulating the transporting and diffusive characteristics of multiple line sources of seeding agents within super-cooled stratus. Several important factors are taken into consideration that affect the diffusion of seeding materials such as effects of topography and vertical wind shear, temporal and spatial variation of seeding parameters and wet deposition. The particles of seeding agents are assumed to be almost inert, they have no interaction with the particles of the cloud or precipitation except that they are washed out by precipitation. The model validity is demonstrated by the analyses and comparisons of model results, and checked by the sensitivity experiments of diffusive coefficients and atmospheric stratification. The advantage of this model includes not only its exact reflection of heterogeneity and unsteadiness of background fields, but also its good simulation of transport and diffusion of multiple line sources.

The horizontal diffusion rate and the horizontal transport distance have been proposed that they usually were difficult to obtain in other models. In this simulation the horizontal diffusion rate is 0.82 m s^{-1} for average of one hour, and the horizontal average transport distance reaches 65 km after 1 h, which are closely related to the background fields.

Key words: Puff trajectory model, Transport and diffusion, Multiple line sources of seeding agents, Heterogeneity and unsteadiness, Diffusion rate and transport distance, Super-Cooled stratus

1. Introduction

Many projects and experiments of rain enhancement are carried out abroad. Most seeded cloud bodies are the convective or topographic clouds. The seeding agents are usually released near their bases and brought into the clouds by the updrafts. Whether the seeding material can reach the areas where cloud liquid water presents is emphasized. Tzivion et al. (1989) demonstrated that effective dispersal of seeding material strongly depends on the seeding altitude and the stage (time) of the development of the cloud. However, it is not that the diffusion of seeding material is not important, but that whether the seeding agents can be brought to seeding altitude by vertical transport is more consequential. Stith et al. (1986) used a gaseous tracer to follow the path of two different AgI cloud aerosols and to discuss the

transport and diffusion in cumulus clouds. A relative dispersion of ice crystals in seeded cumuli was given by Weil et al. (1993). Huston et al. (1991) used the one–dimensional, steady–state and two–dimensional, time–dependent bulk water models to simulate the transport and precipitation development in a seeded cumulus congestus cloud. Bruintjes et al. (1999), after analyzed the renewed optimism regarding the probability of enhancing precipitation using hygroscopic seeding in Mexico, pointed out that some critical problems remain, one of the fundamental impediments is the diffusion and transport of seeding material throughout the cloud.

In China, the projects and experiments of rain enhancement are large–scale. Stratus is the major cloud seeding for rain increment in its northern part. Directly entered by an airplane, the clouds can be seeded. The main concerns of cloud seeding are greatly different between the convective cloud and stratus. The capability of transport and diffusion is focused on whether for stratus or stratiform cloud.

Although the seeded cloud bodies are different, it is essential to learn the temporal and spatial concentration distributions and variations of seeding agents, because it is helpful to understand the complex interactions between microphysical and dynamical processes and between the mesoscale and cloud environment in numerical models. On the other hand, it is beneficial to determine the affecting area, depth and width for assessing operational seeding effectiveness.

One point that should be addressed is related to the disposal of the source and the effects of meteorological fields. With a simple Gaussian plume dispersal method, Gagin and Aroyo (1985) calculated the distance from the target area to the seeding line in order to determine the appropriate locations of the seeding lines with respect to the target areas. Their calculation, however, did not include some important factors that affect the airflow and diffusion of the seeding material. For example, no consideration was given to the effects of topography on the trajectories of the particles, and to the effects of vertical wind shear on diffusion, or to the diurnal and seasonal variations in the wind filed. Having estimated the fraction of seeding material that would manage to reach the proper levels in the clouds, Levin et al. (1997) used a mesoscale model to investigate the effectiveness of broadcast static seeding method in Israel. For simulating the seeding process, the airplane was depicted as a point source moving with a constant speed back and forth along the seeding line.

In the early diffusion model of seeding agents within stratus in China, flow fields were assumed to be homogeneous and steady. Sources were defined as unlimited long line sources, and vertical to wind direction. Coefficients of turbulent diffusion were replaced by their average (Shen et al., 1987). Nonetheless, the actual wind fields and coefficients of turbulent diffusion are functions of time and space, and seeding line sources are limited long and not generally vertical to wind direction due to the restriction of some conditions.

Puff trajectory model is a practical and effective method to present the diffusion of pollutant source. It can deal with the temporal and spatial variation of source parameters with meteorological elements, and can be used to simulate the diffusion of all kinds of scales and sources (Ludwig et al., 1977, 1989; Ludwig, 1982; Sheih, 1978). So it is introduced to simulate diffusion of multiple line sources within stratus. However, it has been proven that the accuracy and efficiency of the model depend on simulating accuracy of flow and turbulence fields. Moreover, a three–dimensional nonhydrostatic mesoscale model has been formulated to simulate the characteristics of dynamics and thermodynamics, which can be input into the puff trajectory model as background fields for improving its accuracy.

Several important factors were taken into consideration that affect the transport and dif-

fusion such as effects of topography and vertical wind shear on diffusion, temporal and spatial variation of seeding parameters and wet deposition. The particles of seeding agents are assumed to be almost inert, they have no interaction with the particles of the cloud or precipitation except that they are washed out by precipitation.

2. The numerical model

The model consists of the three-dimensional nonhydrostatic mesoscale model and the puff trajectory model.

a. *The nonhydrostatic mesoscale model*

1) Basic equations

The governing equations consist of nonhydrostatic prognostic equations of velocity, potential temperature and vapor, and anelastic continuity (see Pielke 1974; Pielke and Martin, 1981 for a detail. Yu et al., 1998). In order to consider accurately topographical effect, a terrain-following vertical coordinate system is used:

$$z^* = h_d(z - Z_g)/(h_d - Z_g) ,$$

where z^* and z are the transformed and Cartesain vertical coordinates, respectively; h_d is the height of model top; Z_g is ground elevation.

The diffusive coefficients are obtained by turbulent kinetic energy (E) and dissipation rate (ε) prognostic equations, which can be written as

$$\frac{D_* E}{Dt} = A + B + D_h\left(\frac{\kappa_{mh}}{\sigma_E}, E\right) + D_v\left(\frac{\kappa_{mz}}{\sigma_E}, E\right) - \varepsilon , \tag{1}$$

$$\frac{D^* \varepsilon}{Dt} = D_h\left(\frac{\kappa_{mh}}{\sigma_\varepsilon}, \varepsilon\right) + D_v\left(\frac{\kappa_{mz}}{\sigma_\varepsilon}, \varepsilon\right) + C_{1\varepsilon}\frac{\varepsilon}{E}\{A - (1 - C_{3\varepsilon})B\} - C_{2\varepsilon}\frac{\varepsilon^2}{E} , \tag{2}$$

$$\kappa_{mz} = C_\mu \frac{E^2}{\varepsilon} , \tag{3}$$

$$A = \left(\frac{h_d}{h_d - Z_g}\right)^2 \kappa_{mz}\left[\left(\frac{\partial u}{\partial z^*}\right)^2 + \left(\frac{\partial v}{\partial z^*}\right)^2\right] , \quad B = \frac{g}{\theta}\left(\frac{h_d}{h_d - Z_g}\right)\kappa_{\theta z}\frac{\partial \theta}{\partial z^*} ,$$

where κ is the diffusive coefficient, its subscriptions m,θ,q,h,z stand for momentum, heat, moisture, horizontal and vertical directions; $\sigma_E,\sigma_\varepsilon,C_{1\varepsilon},C_{2\varepsilon},C_{3\varepsilon},C_\mu$ are empirical constants, respectively. For simplicity, $C_\mu = 0.09$; $\sigma_E = 1.0$; $\sigma_\varepsilon = 1.3$; $C_{1\varepsilon} = 1.44$; $C_{2\varepsilon} = 1.92$; $C_{3\varepsilon} = 1.0$ or 0.0 when stable or unstable (Huang et al., 1989; Ying et al., 1994).

The horizontal and vertical diffusive terms in above equations are

$$D_h(\kappa,\eta) = \frac{\partial}{\partial x}\left(\kappa\frac{\partial \eta}{\partial x}\right) + \frac{\partial}{\partial y}\left(\kappa\frac{\partial \eta}{\partial y}\right) , \quad D_v(\kappa,\eta) = \left(\frac{h_d}{h_d - Z_g}\right)^2 \frac{\partial}{\partial z^*}\left(\kappa\frac{\partial \eta}{\partial z^*}\right) ,$$

where η stands for any scalar quantity.

Difference scheme is employed to solve the equation group, and overnudging iteration is used to solve Possion equation of pressure for its fluctuation.

2) Radiation parameterization

Temperature variations caused by radiation include radiative heating of short wave absorption by water vapor and cooling of long wave radiation.

If there is a cloud, the scheme proposed by Stephens (1978) is adopted. The heating is given by

$$\left(\frac{\partial T}{\partial t}\right)_r = -\frac{[(G-a_w)S_0\cos Z]_{CT}}{\rho C_p}\frac{\partial a_c}{\partial z} \quad , \tag{4}$$

$$G = 0.485 + 0.515[1.041 - 0.16((0.000949p + 0.051)/\cos(Z))^{0.5}] \quad , \tag{5}$$

$$a_w = 0.077(r(z)/\cos(Z))^{0.3} \quad , \tag{6}$$

where $[(G-a_w)S_0\cos Z]_{CT}$ is sum of the direct and diffusive short wave irradiance incident from the cloud top; and a_c the percentage of irradiance transmitting the cloud.

The radiative cooling is defined as follows:

$$\left(\frac{\partial T}{\partial t}\right)_N = \frac{1}{\rho C_p}\left(\frac{\partial \overline{R}_{up}}{\partial z} - \frac{\partial \overline{R}_{dw}}{\partial z}\right) \quad , \tag{7}$$

$$\overline{R}_{up} = \overline{R}_{CB}[1-\varepsilon_{up}] + \varepsilon_{up}\sigma_0\overline{T}^4 \quad , \tag{8}$$

$$\overline{R}_{dw} = \overline{R}_{CT}[1-\varepsilon_{dw}] + \varepsilon_{dw}\sigma_0\overline{T}^4 \quad , \tag{9}$$

where $\overline{R}_{CT}, \overline{R}_{CB}$ are the clear irradiance downward and upward from the cloud top and the cloud base, respectively; $\overline{T}$ is the temperature at the level, ε_{up} and ε_{dw} are the upward and downward effective emissivity.

If there is no cloud, the parameterization refers to the scheme suggested by Mahrer et al. (1977). The heating of the atmosphere by the radiation is given by

$$\left(\frac{\partial T}{\partial t}\right)_r = 0.0231\frac{S_0\cos Z}{\rho C_p}\left(\frac{r(z)}{\cos Z}\right)^{-0.7}\frac{dr}{dz} \quad , \tag{10}$$

where S_0 is the solar constant, Z the zenith, $r(z)$ the optical path length of water vapor above the layer z. It is written as

$$r(z) = \int_z^{H_d} \rho q dz \quad , \tag{11}$$

The radiative cooling at a level N is computed from

$$\left(\frac{\partial T}{\partial t}\right)_N = \frac{1}{\rho C_p}\frac{[R_u(N+1) - R_u(N) + R_D(N) - R_D(N+1)]}{z(N+1) - z(N)} \quad , \tag{12}$$

where the upward and downward fluxes at layer N are given by

$$R_u(N) = \sum_{i=1}^{N-1}\frac{\sigma_0}{2}(T_{i+1}^4 + T_i^4)[\varepsilon(N,i) - \varepsilon(N,i+1)] + \sigma_0 T_s^4[1-\varepsilon(N,0)] \quad , \tag{13}$$

$$R_D(N) = \sum_{i=N}^{H_d-1}\frac{\sigma_0}{2}(T_{i+1}^4 + T_i^4)[\varepsilon(N,i+1) - \varepsilon(N,i)] + \sigma_0 T_{H_d}^4[1-\varepsilon(N,H_d)] \quad , \tag{14}$$

where T_{H_d} and T_s are the temperature at the top of the model and the ground level, respectively; σ_0 is the constant of Stefan—Boltzmann; $\varepsilon(N,i)$ the emissivity between levels N and i.

3) Initial and boundary conditions

Assuming that E, ε are constants in initial time, their initial values can be calculated based on initial profiles of wind and potential temperature.

Lateral boundary conditions are specified as zero gradients.

The conditions imposed at the top of the model are

$$\begin{cases} u_{top} = u_g, v_{top} = v_g, \theta_{top} = \theta_{top0} \\ E = 0.0, \varepsilon = 0.0, \pi' = 0.0, \theta' = 0.0 \end{cases},$$

where π' and θ' are fluctuations of pressure (the Exner function) π and the potential temperature θ.

The bottom boundary is the first layer above the ground, the components of velocity, and the potential temperature can be computed by Businger's profile using the data of the ground and above it. At the ground surface,

$$\begin{cases} E = 5.5u_*^2 + 0.5w_*^2 \\ \varepsilon = \dfrac{u_*^3}{\kappa z \varphi_m} + \dfrac{g(\overline{w'\theta'})}{\theta_{bom}} \end{cases},$$

where $\overline{w'\theta'}$ is the surface heat flux, u_* the friction velocity, w_* the scale of convective velocity (m s^{-1}), φ_m the function of stability. The temperature variation is simply regarded as sinusoidal wave. For the pressure, assuming w_* steady near the surface, neglecting advection and diffusion terms, π' and θ on the ground surface can be obtained by iteration.

b. *The puff trajectory model*

The puff trajectory model presents line sources with a series of discrete puffs moving along the seeding line. In order to consider effect of vertical shear on diffusion, each puff is vertically divided into 7 smaller puffs (sub-puffs). Concentration distribution of each sub-puff agrees with Gaussian diffusive model, its diffusive parameters depend on atmospheric turbulent diffusion on its grid, its movement observes Lagrangian trajectory, and its size is related to atmospheric turbulent diffusion.

At any given time t, $u(t,x',y',z')$, $v(t,x',y',z')$, $w(t,x',y',z')$ are wind speed components at the sub-puff center $(x'(t), y'(t), z'(t))$, after time δt, the position components of each sub-puff will be

$$x_s(t+\delta t) = x'(t) + u(t,x',y',z')\delta t \ , \tag{15}$$

$$y_s(t+\delta t) = y'(t) + v(t,x',y',z')\delta t \ , \tag{16}$$

$$z_s(t+\delta t) = z'(t) + w(t,x',y',z')\delta t \ . \tag{17}$$

Accounting for a reflection of cloud top, the concentration of any sub-puff at any time t can be written as

$$C(t,x,y,z)_{ij} = \frac{Q_j}{(2\pi)^{3/2}\sigma_x^2\sigma_z} \exp\left[-\frac{(x-x_s)^2+(y-y_s)^2}{2\sigma_x^2}\right]\left\{\exp\left[-\frac{(z-z_s)^2}{2\sigma_z^2}\right] + \exp\left[-\frac{(2H-z)^2}{2\sigma_z^2}\right]\right\}, \tag{18}$$

where $i(1,2...7)$ is the ith sub-puff; j is the jth puff; H is the cloud top (m); x,y,z are grid coordinates; Q_j is the amount of AgI particles or the concentration of the ith sub-puff; σ_x, σ_z are the horizontal and vertical diffusive parameters, which can be given by

$$\sigma_x^2(t+\delta t) = \sigma_x^2(t) + 2K_x(t,x_s,y_s,z_s)\delta t \ , \tag{19}$$

$$\sigma_z^2(t+\delta t) = \sigma_z^2(t) + 2K_z(t,x_s,y_s,z_s)\delta t \ , \tag{20}$$

where K_x, K_z are the horizontal and vertical diffusive coefficients.

In calculations, the puff is idealized as a large ellipsoid, which is vertically divided into 7 parts (namely sub-puffs). The concentration of every part can be obtained by ellipsoidal

integration:

$$Q_1 = Q_7 = 0.020Q_T \quad Q_2 = Q_6 = 0.136Q_T \quad Q_3 = Q_5 = 0.220Q_T \quad Q_4 = 0.248Q_T \ ,$$

where Q_T is the concentration or the amount of AgI particles of a puff.

Temporal concentration in a grid point can be calculated by superposing the sub-puff concentration after the position of every sub-puff is determined in simulated domain.

c. *The step of simulation*

In the mesoscale model, the simulation domain whose area is 300 km × 300 km (Fig. 1) is located at Guanzhong region, Shaanxi Province, (33°24′–36°00′N, 107°25′–110°48′E). In this region, the central part is a plain, Qinling Mountains (the tallest point is 3673 m MSL) are to the south, and two plateaus higher than 2000 m are to the west and north. The model top is 6785 m. In horizontal direction, an expanding telescoping grid is used, the grid intervals are symmetry, 10 (5), 6, 5, 4, 3, 2 (31), 3, 4, 5, 6, 10 km (15), the number in the parentheses is the grid point number. Vertically, 20 levels are divided with increasing interval, 25, 60, 100 (5), 200, and 500 m (12). The time step is 20 s. The integration time is 24 h.

In the puff trajectory model, the model domain and top are the same as those for the mesoscale model. Homogeneous grid points 300 × 300 × 25, whose horizontal and vertical grid intervals are 1 km, 200 m, are adopted for concentration calculations. The first layer is the cloud base. The time step is 10 seconds. The integration time is 2 h.

On 31 March 1996, a seeding operation of rain enhancement by aircraft was carried out at 1400 LST. The seeding time is 45 min, and the seeding amount 675 g of AgI, the seeding height 4500 m, where temperature is −6°C and wind at 0800 LST is 18 m s^{-1} (WSW). The heights of the cloud base and top are 1500, 6500 m, respectively. The seeding route is A→B→C→D→E→F→G (Fig. 1), whose length is 327 km. Based on the meteorologically measured surface and sounding data, the simulation begins at 0800 LST, the results of the mesoscale model are output every hour. Fields of wind and turbulence after 1400 LST are input to the puff model by interpolation. The initial positions (X_0, Y_0) of 6 line sources are listed in Table 1. One puff is introduced into the model every 10 s.

The source strength is $675 \times N_r / 45 / 60\ s^{-1} = 0.25\ N_r\ s^{-1}$, where N_r is unit nucleation rate. Here it is disposed as a constant, 10^{13}, which is the corresponding rate at −6°C, not including its variation with temperature (height). The wet deposition rate is taken as $3.7 \times 10^{-5}\ s^{-1}$.

Table 1. Initial positions of 6 line sources

Time	14:15(A)	14:21(B)	14:30(C)	14:39(D)	14:47(E)	14:55(F)	15:00(G)
X_0 (km)	33.4	28.8	67.4	72	119.9	161.3	189.8
Y_0 (km)	142	96.5	144.2	77.6	110.9	149.8	124.2

The simulation includes three parts. The first is to run the mesoscale model to supply the puff trajectory model with the fields of flow and turbulence. The second is to simulate the concentration distributions and variations, and calculate the horizontal diffusive rate and transport distance. The third is to test the sensitivity of temperature stratification and diffusive coefficients.

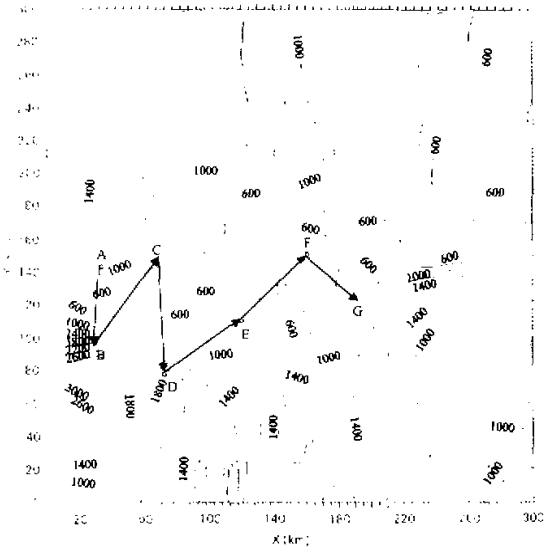

Fig. 1. Topography of simulation domain and seeding route, the arrow stands for the flight direction.

3. Analyses and comparisons of results

The aim of this paper is to mainly study the concentration distributions and variations of seeding agents within stratus.

a. *Results of the mesoscale model*

The comparisons and analyses show that the mesoscale model can satisfactorily simulate the characteristics of dynamics and thermodynamics of atmospheric fields of flow and turbulence (Yu et al., 1997; 1998), which are similar to the other previous simulating results. So this model is feasible to be applied to simulating the transport and diffusion of seeding agents.

b. *Results of the puff trajectory model*

1) The concentration distributions

The horizontal and vertical concentration distributions are shown in Fig. 2. The horizontal cross-sections are on $z = 4500$ m, and the vertical on $y = 130$ km, 140 km before and after 50 min, respectively.

The general features are consistent with the basic theory of diffusion. In the horizontal and the vertical directions, there exist several concentration centers, which lead from the superposition of multiple sources. The diffusive scope increases with time, its horizontal component is greater than that of the vertical, which is caused by the larger horizontal diffusive coefficient.

The concentration center decreases with time. Continuously, its position and the affecting zone move toward the northeast, and together with some degree of distortion and

deformation. It is because that the seeding agents move with upper southwestern wind while they diffuse with turbulent mixing.

The maximum concentrations (hereafter referred to as C_{max} in the following tables) every 10 min beginning at 14:15 LST are displayed in Table 2. Their positions are near newly seeding lines, diffusive ranges are limited due to finite diffusion of newly seeding source, and it diffuses gradually under the influence of background fields. For example, *DE* or *FG* is after 30 or 50 min of seeding (Fig. 2a, 2b). The extreme concentrations decrease with time. The maximum concentrations, in the orders of magnitude, are 10^3 L^{-1} before 40 min (in the course of seeding), 10^2 L^{-1} within 50 min (5 min after seeding), 10^1 L^{-1} after 60 min.

Table 2. Maximum concentrations (L^{-1}) every 10 min

Time	10	20	30	40	50	60	70	80	90	100	110	120
C_{max}	1119.3	1033.6	1285.4	1247.4	526.4	47.2	22.7	14.3	9.6	7.3	6.0	5.1

The diffusive characteristics of multiple line sources can be evidently revealed from the horizontal concentration distributions. The whole seeding line is composed of 6 lines (Fig. 1), each of them corresponds to a line source. Its diffusion, although there exists superposition between them, is typical of line source, not of a point source, which was almost shown in the most previous model of diffusion (Shen et al., 1987, Levin et al., 1997). In addition, the detailed and exact structure of line source can be reproduced in the model. The simulating seeding lines, and the direction and angle of each line source are completely consistent with the real seeding lines. The processes of transport and diffusion of 6 lines are distinct and clear.

The effect of the heterogeneity and unsteadiness of meteorological fields is one of the most important factors considered in the model. Fortunately, we can find out what we had expected from the following results. First, contracting to homogeneity and steadiness, the temporal and spatial concentration variations are irregular. Second, due to the differences of their temporal and spatial positions, which bring out the variations of meteorological fields, the diffusive features of each line source are not similar. Third, the diffusion of every parts of the same line source is also disparate. Forth, in the vertical, they can be revealed from the time evolution of concentration centers. Fifth, the distortion or deformation of isogram such as *BC* and *CD* line sources at 50 min indicates that those effects are stronger than that anywhere else. Last, the variations of horizontal transport distance and diffusion rate (next subsection) also suggest these effects.

The distributions of horizontal and vertical concentrations are more complex and variable with space and time. Gaussian plume model would no longer be suitable for presenting them.

By the comparisons and analyses of the simulating results, we can realize that the model can validly simulate the characteristics of transport and diffusion of multiple line sources under heterogeneous and unsteady conditions.

2) The horizontal transport distance and diffusion rate

In the operation of rain enhancement, the horizontal diffusive rate and the transport distance are useful parameters. The former is usually used to estimate the seeding interval, and the latter is adopted to determine target area, control and buffer region. They are difficult to obtain individually in other models of diffusion, which generally mingle. However, they can be calculated separately in this model.

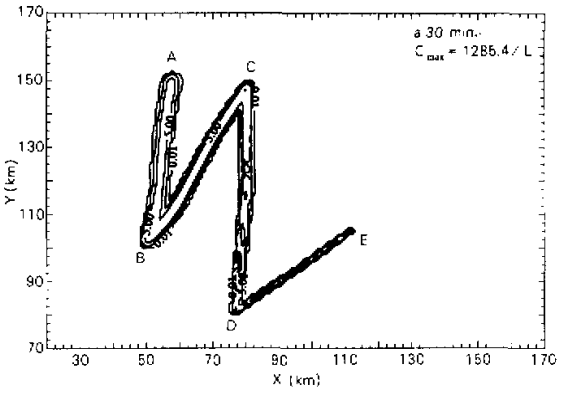
a 30 min.
C_{max} = 1285.4 / L
A
B
C
D
E
Y (km)
X (km)

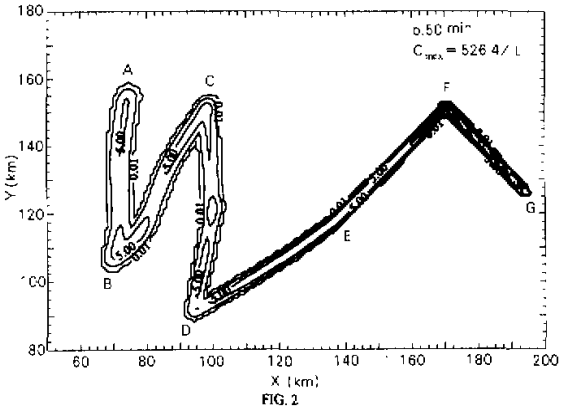
b 50 min
C_{max} = 526.4 / L
A
B
C
D
E
F
G
Y (km)
X (km)

FIG. 2

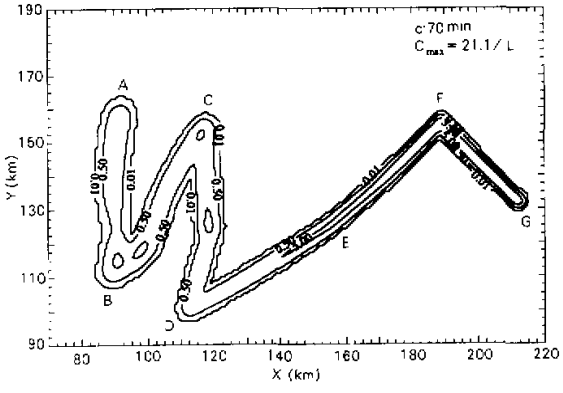
c 70 min
C_{max} = 21.1 / L
A
B
C
D
E
F
G
Y (km)
X (km)

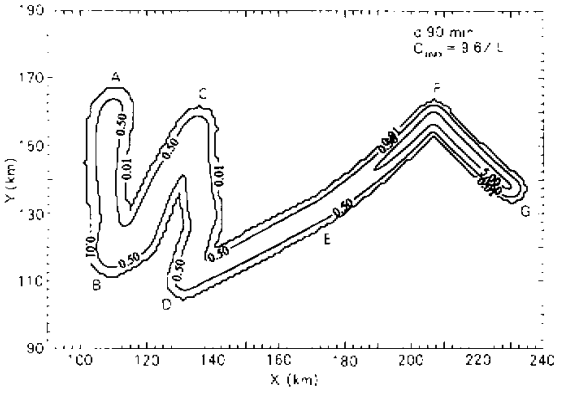

FIG 2

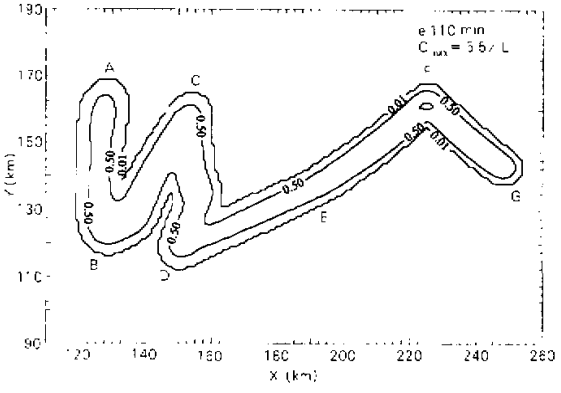

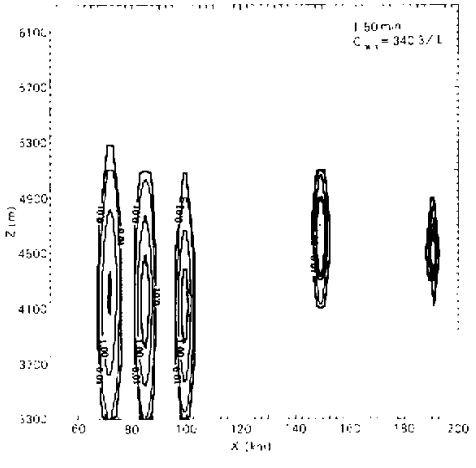

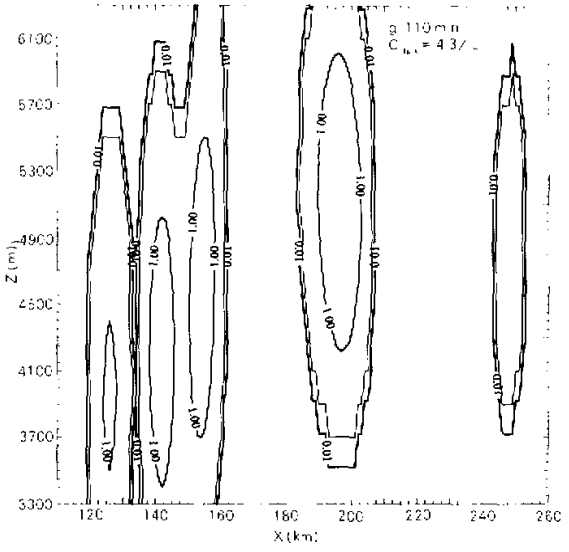

Fig. 2. Horizontal and vertical concentration distributions. (a)–(e) are the horizontal, (f)–(g) the vertical. C_{max} stands for the maximum concentration on this cross-section, not for one at this time. The values of contour lines are 0.01, 0.50, 5.00, 50, 100, 500 L^{-1} in the horizontal, and 0.01, 0.5, 1.00, 5.00, 50, 100, 500 L^{-1} in the vertical. *AB, BC, CD, DE, EF, FG* are 6 line sources.

The time in this section stands for the time that each seeding line enters the cloud.

The middle point of each line source is selected to demonstrate its horizontal transport. The transport distance (R) is obviously related to the upper wind fields. Its maximum (R_{max}), minimum (R_{min}) and average ($\overline{R}$) for every 10 min are shown in Table 3. The variations of horizontal transport distance of 6 line sources with time are shown in Fig. 3. The horizontal transport distance of each source changes with time, and the differences between 6 lines increase gradually, for example, 1.9 km at 10 min and 12.2 km at 60 min. The average transport distance refers to 6 line sources. It reaches 65 km after 1 hour.

Table 3. Maximum, minimum and average of transport distances for every 10 min

T (min)	10	20	30	40	50	60
R_{min} (km)	9.2	18.6	28.1	37.7	47.6	57.8
R_{max} (km)	11.1	22.7	34.6	46.5	58.3	70.0
$\overline{R}$ (km)	10.4	21.2	32.1	43.1	54.1	65.1

The horizontal half width of diffusion (W) is one half of horizontally diffusive width ($3\sigma_x / 2$). The half widths of 270 puffs as well as their maximum (W_{max}), minimum (W_{min}), and average ($\overline{W}$) for every 10 min are shown in Fig. 4 and Table 4. The diffusion of a puff is wavy, and its amplitude obviously increases with time. The puffs numbered 1, 80, 240 diffuse with larger extent, and the puffs numbered 40, 160 narrowly diffuse. The horizontal diffusive rate (V_{Dif}) is the half width of unit time. Its average for every 10 min is also displayed in Table 4.

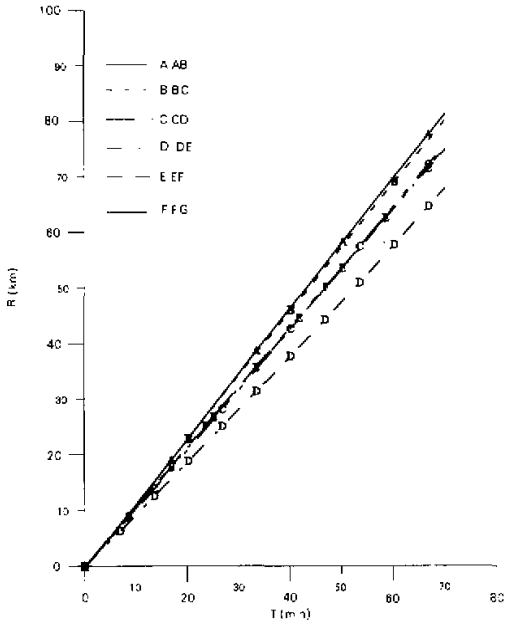

Fig. 3. Transport distances of 6 line sources.

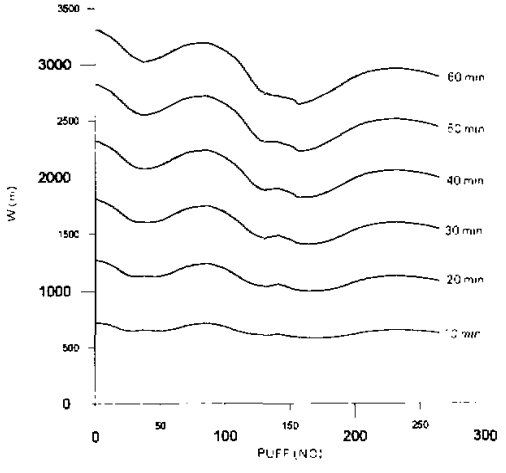

Fig. 4. Half widths of diffusion for 270 puffs.

Table 4. Maximum, minimum and average of half widths and diffusive rate for every 10 min

T (min)	10	20	30	40	50	60
W_{min} (m)	583.9	1001.1	1412.4	1822.8	2234.4	2652.3
W_{max} (m)	722.5	1272.0	1805.8	2321.7	2824.2	3313.8
$\overline{W}$ (m)	644.0	1119.2	1586.8	2049.9	2509.9	2966.9
V_{Dif} (m s^{-1})	1.07	0.93	0.88	0.85	0.84	0.82

The differences between the half widths vary with time, for instance, it increases by 4.8 times from 10 min (138.6 m) to 60 min (661.5 m). The variation of diffusion rate with time is gradually declined, 0.82 m s^{-1} for average of one hour.

It is noted that the simulations done here have no measurement to be compared with and imprudence should be paid to the results. However, the validity of the model can be discussed from a view of simulating characteristics and their values.

In respect to characteristics, the simulating results reflect heterogeneity and unsteadiness distinctly, and reproduce the typically diffusive feature of line source. And the simulating seeding lines agree well with real seeding lines.

With regard to the maximum concentration, the physical assumption of puff separation is that the line source seeding 10 s (1.17 km line length, which is equal to the flying distance in 10 s) is regarded as a point source at a grid point. A puff contains 2.5×10^{13} particles of AgI, the volume of a grid is 0.2 km^3(1 km × 1 km × 0.2 km), so the upper limit of concentration obtained in a gird should be 10^2 L^{-1} (2.5×10^{13} / 0.2 km^3). However, the maximum concentration in the simulation is 10^1 L^{-1} (Table 2). It is equivalent that a puff occupies 0.02 km^3. Namely, the line source about 1 km (1.17 km) diffuses to width and depth of several hundreds and dozens of meters, in stead of filling up the volume of 0.2 km^3 immediately, which is more realistic. The maximum concentrations are 10^2 L^{-1} and 10^1 L^{-1} respectively, in 5 and 15 min after seeding, which suggest that the simulating values are reasonable.

Concerning the average transport distance, 65 km after 1 hour is parallel to 1 hour's transport distance of wind of 18.1 m s^{-1}, which is comparable to the wind at 0800LST at the seeding altitude, 18 m s^{-1}.

Regarding the diffusion rate, 0.82 m s^{-1} for average of one hour is smaller than that in boundary layer and lager than that in the free atmosphere, which coincides with diffusion theory in clouds.

4. Sensitivity experiments

In order to check the simulation validity, we carry out the sensitivity experiments of diffusive coefficients and atmospheric stratification, while the rest conditions keep unchanged.

a. *The atmospheric stratification*

It is generally known that the change of atmospheric stratification will modify the airflow field and alter the turbulent diffusive coefficient. In the stratus clouds, although the vertical distributions and variations at each level of temperature are different and perhaps there exists the isothermal layer or the inversion layer between some levels, the lapse rate of the whole layer generally approaches one of moist-adiabatic process. The lapse rates of −8.0 K / km and −3.0 K / km are tested for its influence.

For different lapse rates, the horizontal and vertical concentration distributions are shown in Fig. 5 and Fig. 6. The configuration of concentration distribution and the variations of diffusive features with time are analogous to the real simulation. For larger (−8.0 K / km) lapse rate or smaller (−3.0 K / km) lapse rate, the scope of the same concentration at a given time is a bit larger or smaller, and the vertical diffusive depth expands or declines, while the diffusive rate increases or decreases slightly. This is because that the increase or decrease of the lapse rate not only intensifies or lessens the strength of turbulence mixing, but also enhances or diminishes the updrafts. This agrees with the basic concept of diffusion. The

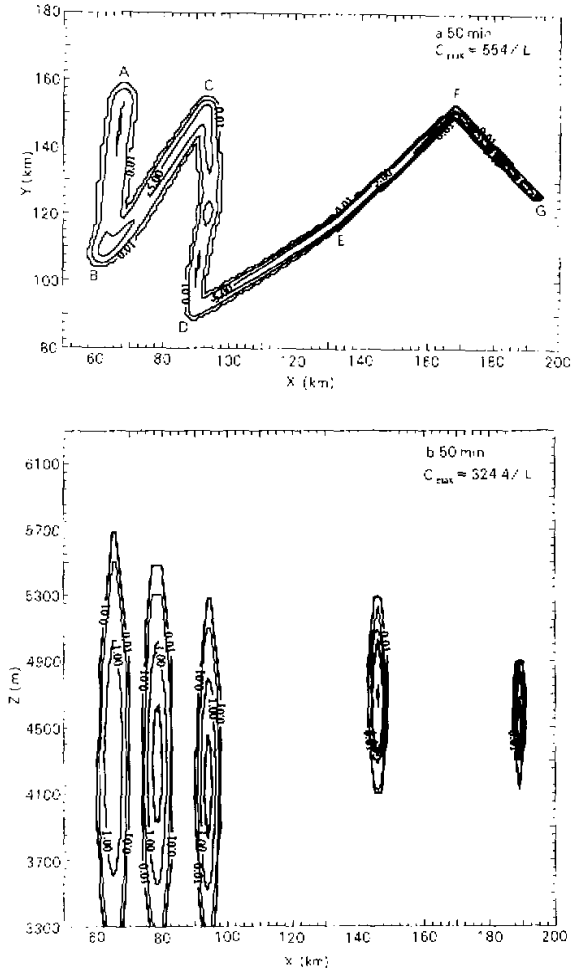

Fig. 5. Horizontal (a) and vertical (b) concentration distributions. The others are the same as in Fig. 2.

maximum concentrations are listed in Table 5. Compared to the corresponding maximum concentrations (Table 2), they increase between 10 and 60 min and decrease after 60 min for larger lapse rate, and increase continuously for smaller lapse rate.

Table 5. Maximum concentrations (L^{-1}) under different lapse rates

Time		10	20	30	40	50	60	70	80	90	100	110	120
−8.0 K / km	C_{max}	1285.3	1143.7	1118.9	1312.3	554.3	52.6	20.3	13.5	8.6	6.4	5.1	4.1
−3.0 K / km	C_{max}	1373.9	1329.3	1447.6	1563.6	605.6	53.7	25.9	16.8	11.2	8.7	7.2	6.2

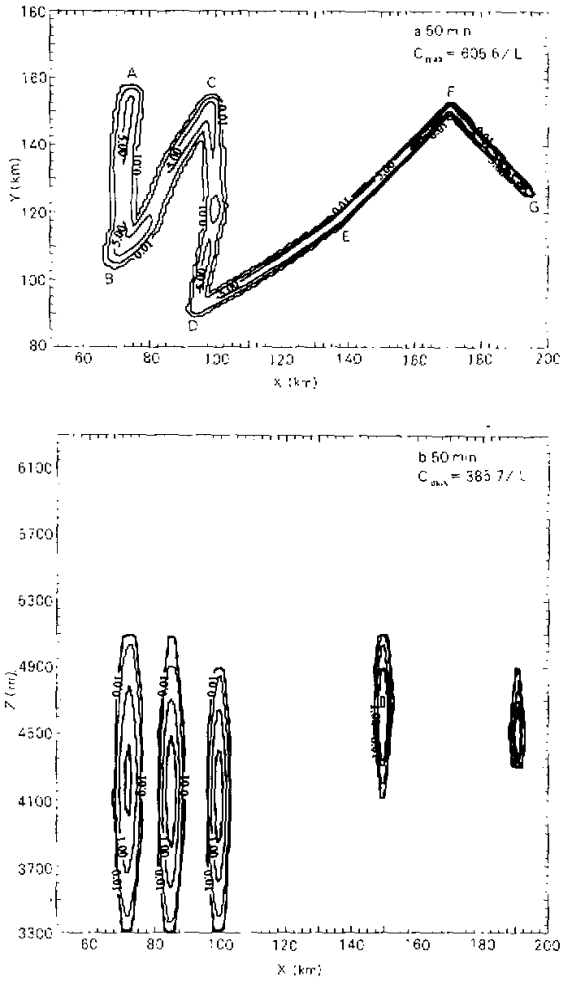

Fig. 6. As in Fig. 5 but for smaller lapse rate.

b. *The diffusive coefficient*

The diffusive coefficient is a sensitive parameter for diffusion. The experiments include enlarging and lessening the coefficient by ten times in horizontal and vertical directions.

For enlarging the coefficient, the concentration distributions are displayed in Fig. 7. The contour also resembles the real simulation, but the extent of the same concentration at a given time is much larger, and the vertical diffusive depth increases obviously while the diffusive rate increases greatly, which cuts the diffusive duration down. Figure 8 presents the experimental results of small coefficient. The extending extent of the same concentration is much smaller simultaneously, but finally it can reach the equivalent scope after some time of

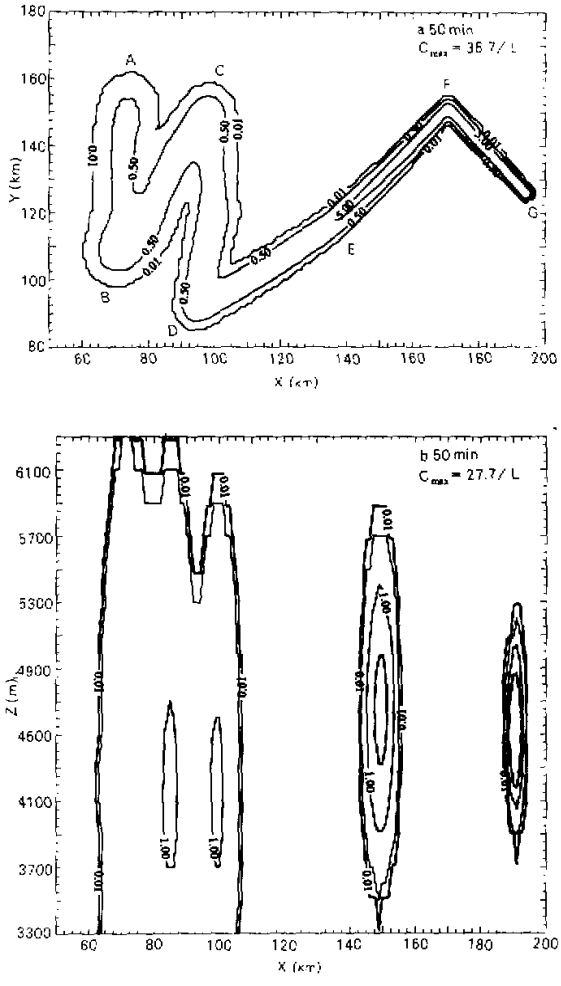

Fig. 7. As in Fig. 5 but for larger coefficient.

transport and diffusion. It is suggested that the reduction of the coefficient, mainly abates the diffusive rate, and has not so much influence on the extending scope of a given concentration, only the required time is rather longer. The variations of diffusive features with time are much slower. Table 6 exhibits the maximum concentrations every 10 min under two conditions, the increment or reduction of the coefficient makes them decline or increase.

The enlargement or contraction of the diffusive coefficient can modify the diffusive rate and the extending scope of the same concentration, it does not affect the scope too much, just shortens or lengthens the diffusive time, and promotes or postpones seeding materials reaching the equivalent scope of the real simulation.

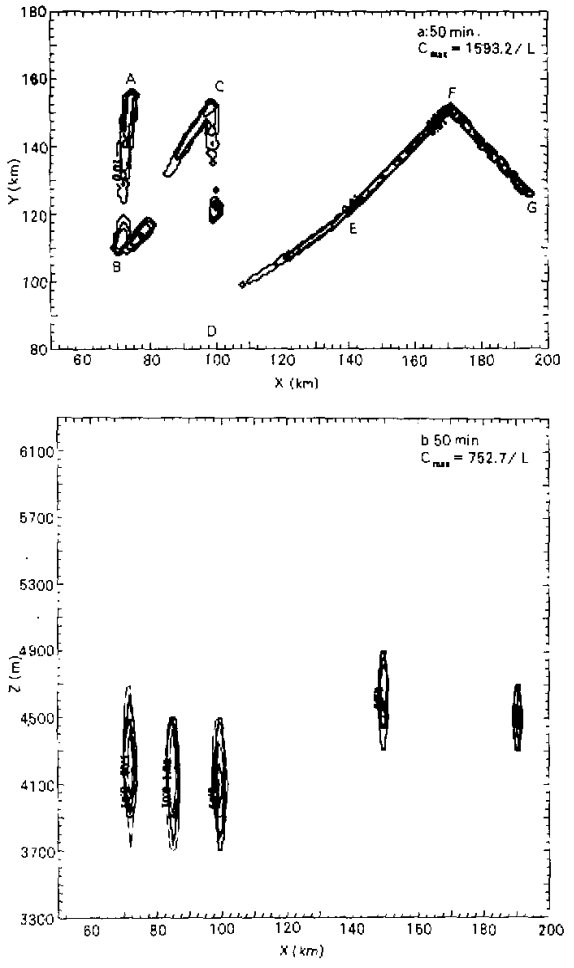

Fig. 8. As in Fig. 5 but for smaller coefficient.

Table 6. Maximum concentrations (L^{-1}) for larger and smaller coefficients

Time	10	20	30	40	50	60	70	80	90	100	110	120
Larger C_{max}	649.9	700.3	564.6	854.4	38.7	6.9	3.0	1.7	1.1	0.8	0.7	0.6
Smaller C_{max}	1726.6	1648.5	1563.8	1888.2	1593.2	440.0	275.9	154.2	75.2	71.4	61.0	53.0

The results of sensitivity experiments indicate that affecting factors are rather sensitive, which can be revealed from the agreement between the simulating results and the basic theory and general characteristics of diffusion.

5. Conclusion

A three-dimensional puff model incorporating a mesoscale nonhydrostatic model has been formulated. Although the interactions between the particles in the cloud and the variation of nucleation rate with temperature were not included, the effects of topography and vertical wind shear on diffusion, temporal and spatial variation of seeding parameters and wet deposition were taken into consideration that affect the transport and diffusion. The model was used to validly simulate the characteristics of transport and diffusion of multiple line sources of seeding agent within stratus. The model can simulate not only the general diffusive features of multiple line sources, but also the subtle differences between every two line sources. The advantage of this model is its good simulation of diffusion of multiple line sources and exact reflection of heterogeneity and unsteadiness of background fields.

The model results show that the general diffusive features of multiple line sources of seeding agent are consistent with basic theory of diffusion, but more complex and variable with space and time, compared to diffusion of vertical line source under the homogeneous and steady condition. Gaussian plume model would no longer be suitable for presenting concentration distribution.

The heterogeneity and unsteadiness can be evidently revealed from the temporal and spatial concentration variations, the differences of diffusive features of each line source and its every parts. Besides, the time evolution of concentration centers in the vertical, and distortion or deformation of isogram as well as variations of the half width also can reflect their effects.

The quantification of diffusion rate and average transport distance has been proposed to determine the horizontal diffusivity and transport distance, which usually were difficult to obtain in other models. However, they are closely relared to the background fields. The diffusion rate is 0.82 m s^{-1} for average of one hour, and the average transport distance reaches 65 km after 1 hour in our simulation.

The sensitivity experiments of diffusive coefficients and atmospheric stratification are designed to check the simulation validity and efficiency. The results suggest that the influence factors are rather sensitive.

REFERENCES

Brunties, R. T., G. L. Kok, D. W. Breed, and V. Salazar, 1999: Hygroscopic seeding: theory and practice. Seventh WMO scientific conference on weather modification, WMO / TD-No. 936, 65-68.

Gagin, A., and M. Aroyo, 1985: Quantitative diffusion estimates of cloud seeding nuclei released from airborne generators. *J. Wea. Mod.*, **17**, 59-70.

Huang, C. Y., and S. Raman, 1989: Application of the E-ε closure model to simulations of mesoscale topographic effects. *Bound. Layer Meteor.*, **49**, 169-195.

Huston, M. W., A. G. Detwiler, and F. J. Kopp, 1991: Observations and model simulations of transport and precipitation development in a seeded cumulus congestus cloud. *J. Appl. Meteor.*, **30**, 1389-1406.

Levin, Z., S. O. Krichak, and T. Reisin, 1997: Numerical simulation of disposal of inert seeding material in Israel using a three-dimensional mesoscale model. *J. Appl. Meteor.*, **36**, 474-484.

Ludwig, F. L., L. S. Gasiorek, and R. E. Ruff, 1977: Simplification of a Gaussian puff model for real-time minicomputer use. *Atmos. Environ.*, **11**, 431-436.

Ludwig, F. L., 1982: Effect of a change of atmospheric stability on the growth rate of puffs used in plume simulation models. *J. Appl. Meteoro.*, **21**, 1371-1374.

Ludwig, F. L., R. Salvador, and R. Bornstein, 1989: An adaptive volume plume model. *Atmos. Environ.*, **23**,

127–138.

Mahrer, Y., and R. A. Pielke, 1977: The effects of topography on the sea and land breezes in a two-dimensional numerical model. *Mon. Wea. Rev.* **105**, 1151–1162.

Pielke, R. A., 1974: A three-dimensional numerical model of the sea breezes over south Florida. *Mon. Wea. Rev.*, **102**, 115–139.

Pielke, R. A., and C. L. Martin, 1981: The derivation of a terrain-following coordinate system for use in a hydrostatic model. *J. Atmos. Sci.*, **38**, 1707–1713.

Shen Yiming, and Chen Jihang, 1987: Numerical solution to the problem on diffusion of catalytic agent released from an airplane. *Acta Meteorologica Sinica*, **1**, 190–197.

Sheih, C. M., 1978: A puff pollutant dispersion model with wind shear and dynamic plume rise. *Atmos. Environ.*, **12**, 1933–1938.

Stephens, G. L., 1978: Radiation profiles in extended water clouds. II: Parameterization schemes. *J. Atmos. Sci.*, **35**, 2123–2132.

Stith, J. L., D. A. Griffith, R. L. Rose, J. A. Flueck, J. R. Miller, Jr., and P. L. Smith, 1986: Aircraft observations of transport and diffusion in cumulus clouds. *J. Climate Appl. Meteor.*, **25**, 1959–1970.

Tzivion, S., T. Reizin, Z. Levin, G. Feingold, and A. Manes, 1989: Dispersion of seeding material in clouds. *Pro. Fifth WMO Scientific Conference on Weather Modification and Applied Cloud Physics*, Beijing, China, World Meteor. Org., 171–174.

Weil, J. C., and R. P. Lawson, 1993: Relative dispersion of ice crystals in seeded cumuli. *J. Appl. Meteor.*, **32**, 1055–1073.

Ying, R., V. M. Wilson, and R. M. Ypma, 1994: Numerical simulation of flow data over two-dimensional hills. *Bound. Layer Meteor.*, **70**, 401–427.

Yu Xing, Fan Peng, Wang Xiaoling, Dai Jin, and Li Zhaoyuan, 1998: Numerical simulation of multiple line source diffusion of seeding agents within stratiformis. *Acta Meteorologica Sinica*, **56**, 708–723 (in Chinese).

Yu Xing, Wang Xiaoling, Dai Jin, Yang Wenfeng, and Li Zhaoyuan, 1997: Numerical simulation of boundary layer structure within complex topography. *Plateau Meteorology*, **16**, 389–401 (in Chinese).